Inferring thermospheric composition from ionogram profiles: A calibration with the TIMED spacecraft

Christopher J. Scott[1], Shannon Jones[1], Luke A. Barnard[1]

[1]Department of Meteorology, University of Reading, Reading, RG6 6BB, UK

5 *Correspondence to*: Christopher J. Scott (chris.scott@reading.ac.uk)

Abstract. Measurements of thermospheric composition via ground-based instrumentation are challenging to make and so details about this important region of the upper atmosphere are currently sparse. We present a technique that deduces quantitative estimates of thermospheric composition from ionospheric data, for which there is a global network of stations. The visibility of the F1 peak in ionospheric soundings from ground-based instrumentation is a sensitive function of 10 thermospheric composition. The ionospheric profile in the transition region between F1 and F2 peaks can be expressed by the 'G' factor, a function of ion production rate and loss rates via ion-atom interchange reactions and dissociative recombination of molecular ions. This in turn can be expressed as the square of the ratio of ions lost via these processes. We compare estimates of the G factor obtained from ionograms recorded at Kwajalein (9ºN, 167.2º E) for 25 times during which the TIMED spacecraft recorded approximately co-located measurements of the neutral thermosphere. We find a linear relationship between 15 $\sqrt{G}$ and the molecular: atomic composition ratio, with a gradient of 2.23 ±0.17 and an offset of 1.66 ± 0.19. This relationship reveals the potential for using ground-based ionospheric measurements to infer quantitative variations in the composition of the neutral thermosphere. Such information can be used to investigate spatial and temporal variations in thermospheric composition which in turn has applications such as understanding the response of thermospheric composition to climate change and the efficacy of the upper atmosphere on satellite drag.

20 **1 Introduction**

A small fraction of the Earth's upper atmosphere, the thermosphere, is ionised principally by solar extreme ultra violet and x-ray radiation to form the ionosphere. Continuous measurements of the Earth's ionosphere have been made since the early 1930s (e.g. Gardiner et at, 1982) exploiting the fact that ionisation reflects high frequency (HF) radio waves. In this way, detailed records have been obtained of the long-term variation of the ionosphere in response to changes in season, solar activity, 25 space weather events and phenomena such as solar eclipses. Initiatives such as the International Geophyscial Year in 1957 enabled a comprehensive global coverage of routine ionospheric measurements that, despite some decline in the number of observing stations, continues to date.

While the ionosphere makes up only a small fraction (~0.01%) of the upper atmosphere, measuring the neutral thermosphere is more challenging. Ground-based measurements of the thermosphere have been made via optical detection of atmospheric airglow from which temperature and winds can be inferred (e.g. Burnside et al, 1982; Meriwether et al, 1983; Griffin et al, 2008). Though too high for conventional weather balloons, in-situ measurements of thermospheric composition, temperature

5 and winds have been made using sub-orbital rockets, usually conducted on a campaign basis, which provide only a highly localised snapshot of thermospheric conditions (e.g. Spencer and Carignan, 1988). More recently earth-orbiting spacecraft such as the Thermosphere Ionosphere Mesosphere Energetics and Dynamics (TIMED) spacecraft (Kusnierkiewicz, 2003) have made measurements of thermospheric composition, temperature and winds from orbit. Such measurements can build up a global picture of the thermosphere with maps composed from measurements made over many orbits. In 2018 the Global

10 Observations of the Limb and Disk (GOLD) instrument (Eastes et al, 2017), hosted by the STS-14 commercial spacecraft, was launched into a geostationary orbit from where it makes measurements of the thermosphere over an entire hemisphere.

Despite the challenges in measuring the neutral upper atmosphere, it is desirable to do so since the thermosphere directly impacts modern technology such as via frictional drag on spacecraft and, through its influence on the ionosphere, radio

15 communications and the accuracy of Global Navigation Satellite Systems (GNSS). Thermospheric composition measurements are also needed to understand the seasonal variation of the ionosphere (e.g. Rishbeth and Setty 1961; King, 1961b; Rishbeth and Kervin, 1968) which differ with geographic location and have been shown to exhibit long-term changes (Bremer, 2004; Scott, Stamper and Rishbeth, 2014; Scott and Stamper, 2015).

20 Modelling work by Roble and Dickinson (1989), indicated that the Earth's upper atmosphere would be expected to cool by around 30-40K in response to greenhouse trapping in the lower ionosphere. Subsequent work by Rishbeth (1990) and Rishbeth and Roble (1992) extended this work to consider the effects on the ionosphere. They predicted that the height of the ionospheric F2 layer would decrease by around 15km. Subsequently Bremer (1992) presented data from Juliusruh (54.6°N, 13.4°E) which supported this hypothesis though a comprehensive analysis of one hundred ionospheric stations (Bremer, 2004) indicated that,

25 for the F2 region at least, such long-term change varied with location, a result which was attributed by the author to F region dynamics and the inhomogeneity of the datasets. Scott and Stamper (2015) have shown that the global variation in long-term changes to the height of the F2 region is similar to that observed for long-term change observed in the seasonal variation of F2. Since the latter is determined by changes in thermospheric composition, they suggest that this could also explain the regional variation in the trends observed in F region heights.

30

Given the potential applications for measurements of the neutral thermosphere, and the influence this has on the ionosphere, it is desirable to investigate whether the ionospheric measurements can be used to measure the thermosphere by proxy. In this paper we investigate the potential for using the shape of the ionospheric profile measured by ground-based instrumentation to

infer the change in thermospheric composition with height. A comparison with co-located measurements of the thermospheric composition from the TIMED spacecraft enables some check on the efficacy of this process.

2 Theoretical background

Ions and electrons within the ionosphere exist in a state of dynamic equilibrium, with ions being produced by photoionisation
5 and lost through recombination. Which particular loss process dominates depends on the composition of the background thermosphere. The atmosphere above the turbopause at around 100km becomes sufficiently tenuous that the gasses are no longer mixed through collisions and each gas species diffuses into a hydrostatic equilibrium according to its molecular or atomic mass. Heavier molecules such as N_2 and O_2 dominate at lower thermospheric altitudes (around 100km) while atomic oxygen, O, becomes the dominant neutral species at greater altitudes (around 300km).

10

Early work on the ionospheric continuity equation (Rishbeth and Garriott, 1969, and references therein) for the concentration of electrons, N, atomic ions N_{A+} and molecular ions N_{M+} assumed that molecular ions in the lower thermosphere were lost through dissociative recombination while the ion-atom interchange reaction occurring at F2 altitudes where O^+ ions dominate, involved interaction with a molecular gas, of concentration n[M]. This process is thought to dominate in the upper
15 thermosphere since molecular ions produced by photo-ionisation are rapidly removed by dissociative recombination. Given these assumptions, it was possible to write the continuity equations for N, N_{A+} and N_{M+} as;

$$\frac{dN}{dt} = q - \propto NN_{M+} \tag{1}$$

20 $$\frac{dN_{A+}}{dt} = q - \gamma n[M]N_{A+} \tag{2}$$

$$\frac{dN_{M+}}{dt} = \gamma n[M]N_{A+} - \alpha NN_{M+} \tag{3}$$

with charge neutrality requiring that;

$$N = N_{A+} + N_{M+} \tag{4}$$

25 where q is the ion production rate, α is the 'square law' loss coefficient associated with dissociative recombination and γn[M] is the loss coefficient for atomic ions through ion-atom interchange. Assuming equilibrium conditions (d/dt=0) and writing β=γn[M], the ratio of atomic and molecular ion concentrations can then be written;

$$\frac{N_{A+}}{N_{M+}} = \alpha N/\beta \tag{5}$$

30

Using equation (5) to substitute for $N_m{}^+$ in equation (1) and similarly substituting for $N_A{}^+$ from equation (2), a quadratic expression for the electron concentration can be obtained.

$$\alpha\beta N^2 - \alpha qN - \beta q = 0 \qquad (6)$$

5

The positive root of this equation gives the expression;

$$N = \left(\frac{q}{2B}\right)\left[1 + \left(1 + \frac{4\beta^2}{\alpha q}\right)^{\frac{1}{2}}\right] \qquad (7)$$

10   This reduces to

$$N = N_\alpha = \left(\frac{q}{\alpha}\right)^{\frac{1}{2}} \; if \; 4\beta^2 \gg \alpha q \qquad (8)$$

and

15   $$N = N_\beta = \frac{q}{\beta} \; if \; 4\beta^2 \ll \alpha q \qquad (9)$$

Ionospheric layers embedded within the thermosphere therefore undergo different loss processes. At E-region altitudes, around 100 km, the dominant neutral species are molecular, and so equation (8) dominates which results in rapid recombination (~ seconds) for a given ion. This reaction is fast because it is not restricted to a specific relative energy between the ions and electrons since any additional energy breaks the molecular bonds, generating atomic neutrals. This dissociative recombination of ionisation associated with molecular gasses is rapid compared with the loss at higher F-region altitudes (around 300km) where neutral atomic oxygen dominates. Recombination with atomic oxygen either requires a third body in the collision to absorb any excess kinetic energy or that the electron and ion have specific energies that enable an electron to be captured by the ion. Consequently, such reactions are much slower than loss of ionisation through dissociative recombination. Atomic ions can also undergo charge-exchange reactions with molecular neutrals, with the resulting molecular ions rapidly recombining. As a consequence, equation (9) applies with atomic oxygen ions tending to dominate in the upper ionosphere under equilibrium conditions.

Given these two regimes, there must be an altitude at which the equilibrium reaction transitions between the domains of the αN^2 and the βN loss processes. This occurs in the lower F region, where the peak level of F-region ion production occurs. Ratcliffe (1956) demonstrated that this could account for the splitting of the F layer into the F1 and F2 components.

From equation (7) it can be determined that the parameter $\beta^2/\alpha q$ determines the shape of the height profile in electron concentration. Defining G as the value of this parameter at the level of peak production, and using equations (8) and (9) it is possible to show that;

$$5 \quad G = \frac{\beta^2}{\alpha q} = N_\alpha^2 / N_\beta^2 \qquad (10)$$

If K is defined as the ratio of scale heights of the ionisable gas and the linear loss coefficient, β, K depends on the molecular gas involved in the ion-atom interchange (O_2 or N_2). Since the dominant ionisable gas is atomic oxygen, K=28/16 =1.75 for N_2 and 2 for O_2 if β is assumed to be independent of temperature.

10

If G and K are constant, changes in q and β can affect the magnitude and vertical position of the electron concentration height profile, but do not affect its shape.

Figure 1 (after figure 28, Rishbeth & Gariott, 1969) presents the vertical profile of electron concentration for a range of values

15 of G. For low values of G the transition is smooth, with a large ledge appearing for G=4 which becomes more pronounced for larger values of G.

Between F1 and F2 layers a transition occurs from a thermosphere that is predominantly molecular to one where neutral atomic oxygen dominates, with the dominant loss process changing from the square law loss coefficient α to the linear loss coefficient

20 β. The exact nature of this transition has a marked impact on the visibility of the F1 peak observed in vertical profiles of ionospheric electron concentration as measured by ionospheric sounders, with such a ledge resulting in a prominent 'cusp' for G > 1.

Rishbeth and Kervin (1968) conducted a qualitative assessment of changes to the G parameter for three stations; Anchorage,

25 Washington and Grand Bahama. They observed a seasonal change in G which followed the expected behaviour in ionospheric production rate, q, when corrected for solar zenith angle and sunspot number. They concluded that β was the most likely factor to be causing the observed changes which in turn suggests a variation in thermospheric composition or temperature. Changes in thermospheric composition are also consistent with observations of the F-region seasonal anomaly (Rishbeth and Seti, 1961; King 1961b; King, 1970).

30 **3 Ground-based ionospheric monitoring- the ionosonde**

Since the early 1930s, routine observations of the distribution of ionisation with height in the Earth's atmosphere have been undertaken using ionospheric sounders known as ionosondes (Gardiner et al, 1982). These ionosondes rely on the fact that a

radio signal transmitted vertically will be returned from an altitude at which the local plasma concentration matches the frequency of the transmitted radio pulse. The electron concentration, N, (m^{-3}) is related to the radio frequency, f, (Hz) by the relation;

5   $f = 8.98\sqrt{N}$ (11)

Typical electron concentrations within the Earth's ionosphere correspond to radio frequencies in the high frequency (HF) waveband ~ 0.5 – 20 MHz. By transmitting a range of radio frequencies and assuming that the radio pulses are travelling at the speed of light in a vacuum, a height profile of the electron concentration in the ionosphere can be estimated from the time

10 of flight versus radio frequency. Such a plot is referred to as an ionogram. Since the radio pulses are not travelling through a vacuum but a weakly ionised medium, their time-of-flight is extended through interaction with the local plasma. The heights on an ionogram are therefore referred to as virtual heights, h', which are greater than the equivalent true heights, h, depending on the amount of ionisation through which the pulse has had to travel. As the transmitted radio frequency approaches the resonant plasma frequency at the peak of an ionospheric layer it is further delayed by its resonance (frequent

15 absorption and re-emission by the local electrons) and the time of flight becomes effectively infinite. This leads to distinct cusps on an ionogram at the peak frequency of each layer (see example in figure 2). Such critical frequencies are denoted foE, foF1, foF2 for the E, F1 and F2 layers respectively and have long been used to represent the peak frequency returned by the layer, and via equation 11, the peak electron concentration. As detailed above, the visibility of the foF1 cusp in ionograms is controlled by the G parameter, which in turn is determined by the thermospheric composition in the transition

20 region between the F1 and F2 layers.

3.1 Estimating values of G from an ionogram

Analysis of the F1-F2 transition region was instigated by King (1961), in which the ionospheric electron concentration profile was compared with a set of theoretical curves derived for a range of values of G. This work demonstrated that it was possible to determine relative changes in G throughout the day, from which changes in thermospheric composition could be inferred.

25 This technique was further elaborated (King and Lawden, 1964) to one in which templates were produced and matched with ionospheric profiles. The curves on these templates were created assuming a constant scale-height, H_v, of 30 km at the bottom of the transition region and a vertical scale height gradient, Γ, that varied with reduced height, Z, as $H_O=H_v exp(-\Gamma Z_v)$. These templates, produced for a range of values of Γ and G were compared with each ionospheric profile and the template that best matched the curve was used to identify the associated values of Γ and G. Rishbeth and Kervin (1968) used a similar technique

30 to investigate the diurnal and seasonal variation of G from which they inferred changes to the neutral thermospheric composition or temperature.

Lawden (1969) subsequently investigated problems associated with the assumptions made in producing the templates, namely that the ionisation was assumed to be entirely O^+, that the ionising radiation was monochromatic and that the loss rate, β, was inversely proportional to the temperature. He concluded that the relative production rates of N_2 and O was very important, as was any temperature variation in the reaction rates. King (1969) addressed the validity of these assumptions and concluded

5   that the assumptions were indeed adequate for expressing the shape of the F1 region quantitatively.

The purpose of this paper is to apply the method of King and Lawden (1968), as used by Rishbeth and Kervin (1968) to modern ionogram traces so that estimates of G can be made. Instead of producing templates however, a best-fit curve was found by minimising the residuals between the data and model profiles within the transition region of each ionogram. This method is

10   largely the same as used previously except that neither the initial scale height nor the foE/foF1 ratio were fixed.

The production and loss functions in the ionospheric profile are;

$$q = q_o \exp[(1 + \Gamma)(1 - z - e^{-Z})] \tag{11}$$

15   $$L = \beta n / \left(1 + \frac{\beta}{\alpha N}\right) \tag{12}$$

where

$$\beta = \beta_o \exp[-(k + \Gamma)z] \tag{13}$$

Assuming equilibrium, q = L, these equations can be used to form a quadratic expression in $N\sqrt{(\alpha/q)}$;

20

$$\left(N\sqrt{\alpha/q}\right)^2 - \left(N\sqrt{\alpha/q}\right)\sqrt{q\alpha/\beta^2} - 1 = 0 \tag{14}$$

Adopting the practice of Rishbeth and Kervin (1968), we define H_1 as the scale height of atomic oxygen at the peak of ion production for the layer, but rather than estimating the scale height profile assuming a constant vertical gradient, $\Gamma = dH/dh$, we

25   instead adopt the practice of King and Lawden (1964) in which the scale height gradient varies exponentially with reduced height although we take the reference scale height, H_1, at the peak of the F1 layer. Unlike these authors, we include H_1 as a variable during our fitting process. We also assume that N_2 is the dominant molecular neutral species so that K=1.75. Since we have no prior information about the temperature profile, we adopt the assumption of these earlier analyses that the loss rate, α, is assumed to vary inversely with temperature and therefore H.

30

In order to produce templates, Rishbeth and Kervin (1968) also assumed a fixed ratio between foE and foF1 (by inspection of a long time series of data from the station under study). This was to enable a reasonable estimate of the curve at the lower end of the transition region. Since we are carrying out a best-fit, we allow this to be a variable in our analysis.

Having estimated the ionospheric profile in the transition region, we use the critical frequency of the E-region to produce a simple model of the E-region represented as a 10km thick slab of ionisation at the height of the E-layer (assuming h'E≈hmE). Since we have no information about the ionisation within the E-F valley, we initially assume a true height of 200 km for the F1 layer and include a variable offset, *h_offset*, which is used to best match the difference in virtual height between the E and F1 layers.

Having created an ionospheric height profile, this then needs to be converted to virtual height for comparison with each ionogram. The virtual height, h', and the true height, h, are related by the integral;

$$h'(f) = \int_0^f \mu'(dh/df_N)df_N + h(0) \tag{15}$$

Where $h(0)$ is the height at the base of the ionosphere below which it is assumed that $f_N=0$ and μ' is the group refractive index, a complex function of plasma and gyro frequencies derived from the Appleton Hartree equation (e.g. Storey, 1959; Rishbeth and Garriott, 1969). This process therefore requires an estimate of the magnetic field, B, for which the International Geomagnetic Reference Field (IGRF, Thébault et al, 2015) was used for the time and location of each measurement.

3.2 Analysis of the ionogram data

To compare the model ionogram with real data, first some parameters (foE, h'E and the frequencies corresponding to h'F1 and h'F2) need to be scaled from the ionogram data and used as input to the ionogram model. These parameters remain fixed throughout the fitting process. Having created a model ionogram using default initial input parameters ($\Gamma_1=0$, G=1, $H_1=300$ km, foF1=foE/0.7 and h_offset = 0), the model and data-derived ionogram traces are compared and the differences between the two curves within the transition region (between two frequencies denoted by the lowest virtual height of the F1 and F2 layers) was used to calculate a mean square residual. The input parameters are then iterated to minimise this residual and the resulting 'best-fit' parameters stored. Despite there being five input parameters, each affects the profile in different ways. The main influence of varying Γ_1 is to affect the difference in virtual height between the F1 and F2 layers. Varying the G parameter, as expected, alters the visibility of the F1-F2 transition, H_1 affects the fit to the F1 profile and h_offset adjusts the height between the E and F1 layers. Having ascertained the input parameters that resulted in the best fit to the data, uncertainties in G and H_1 were estimated by iterating these values until the mean square residual was doubled. The four parameters are not completely independent however and there are many local minima within the fitting surface. Automated minimisation techniques tended to find a local minimum closest to the initial model parameters and so for the purposes of this demonstration, the minimum residual was determined by manual inspection and iteration. This manual check ensured that the minimum difference between model and data ionograms best represented the shape of the curve around the F1-F2 transition. While it is

highly desirable to automate this part of the process, tests showed that independent manual fitting of the same ionograms obtained results that were within the quoted uncertainties. Assuming the ionisation profile is predominantly composed of O^+ ions, and that the ion and neutral temperatures were the same, the value of H_1 can then be used to estimate the temperature at the F1 peak since $H=kT/mg$, where k is Boltzmann's constant, T is the ion temperature, m is the ion mass and g the acceleration

5   due to gravity.

4 Thermospheric Profiles from the TIMED Spacecraft

Data from the Global Ultra-Violet Imager (GUVI, Yee et al, 2003) on board the Thermosphere Ionosphere Mesosphere Energetics and Dynamics (TIMED) spacecraft (Kusnierkiewicz, 2003), were used for comparison with the ground-based ionospheric parameters derived in this study. This mission, launched in December 2007 was designed to study the ionospheric

10   and neutral atmosphere interactions in the mesosphere and lower thermosphere. The TIMED spacecraft carried four remote-sensing instruments, in a circular Earth orbit at an altitude of 625 km with an inclination of 74.1°. The four instruments are; GUVI, a cross-track scanner measuring spatial and temporal variations of temperature and thermospheric gas concentrations in the lower thermosphere; The Solar Extreme ultraviolet Experiment (SEE) which measures solar radiation; The Sounding of the Atmosphere using Broadband Emission Radiometry (SABER), measuring infra-red emissions below 120 km and the

15   TIMED Doppler Imager (TIDI) measuring wind direction and speed.

4.1 The Global Ultra-Violet Imager

The GUVI instrument is a scanning spectrograph sensitive to emissions in the far ultraviolet region (115 -180 nm) of the electromagnetic spectrum. It was designed to detect airglow emissions in the Earth's upper atmosphere. Within this region of the spectrum there are strong emissions from atomic hydrogen, (H) at 121.6 nm; atomic oxygen (O) at 130.4 and 135.6 nm

20   and molecular nitrogen (N_2) at 165 and 185 nm. Absorption by molecular oxygen (O_2) occurs across the spectrum and this must be accounted for in determining O and N_2 concentrations (Meier et al, 2015). The GUVI instrument has a field of view of 11.78° and used a mirror to sweep this through an arc up to 140° perpendicular to the spacecraft orbit with a spatial resolution of around 8km. After 10 million such scans, the mirror failed in 2007. The instrument continues to operate in a fixed look direction, at about 47° from nadir. When scanning was possible, three regions were typically monitored during each orbit; the

25   daytime low-to-mid latitude thermosphere, the night time low-to-mid latitude thermosphere and the high latitude auroral zone.

Of interest for this study are thermospheric composition and temperature profiles derived from limb observations using GUVI data (Meier et al, 2015). Due to the nature of the orbit and varying solar activity, these measurements are made under a range of solar illumination and solar and geomagnetic conditions. In order to estimate altitude profiles of the individual gas species,

30   careful calibration is required before the nonlinear relationships between emission rates and number densities can be deconvolved. There is insufficient information to employ tomographic inversion techniques, and so additional information from the NRLMSISE-00 model was used to constrain the extraction of geophysical parameters from the column emission

rates. The technique is robust for measurements made at locations with latitudes below 60º (to avoid auroral contamination) and with a solar zenith angle less than 80º. Data from the epoch 2002-2007 have been analysed in this way and are made available at http://guvitimed.jhuapl.edu/data_products. These data products are subject to ongoing updates as resources allow. Each file contains data detailing the vertical profiles of thermospheric temperature and the concentrations of the neutral

5   constituents N_2, O_2 and O below 310 km. While each profile represents a line-of sight view through the airglow emission profile, it is assumed that there is no horizontal variation (an assumption that is most appropriate for lower latitudes) and the location of a given profile is defined as the tangent point at the peak of the airglow layer, around 160km.

While the location of the spacecraft at any given time can be determined from the online data archives, the location assigned

10   to each of the limb observations is stored within each file. At the time of writing, this required each data file to be examined in order to determine the location and timing of such measurements. In order to enable rapid comparison with ground-based measurements, a database was created containing the geographic location of all limb scans within the dataset. It was subsequently possible to determine the times at which measurements were being made in the vicinity of ground-based ionospheric monitoring stations for which data were available via the Global Ionospheric Radio Observatory (GIRO; Reinisch

15   and Galkin, 2011). While the coincidence of observations is a function of the timing of both spacecraft and ionospheric observations, the nature of the spacecraft orbit meant that there were far more overpasses for low-latitude ionospheric monitoring stations than for those at high latitudes. Since the purpose of this study is to look at any potential correlation between satellite measurements of thermospheric densities and the shape of ground-based ionospheric profiles, it is advantageous to use measurements far from the auroral zones and their associated geomagnetic activity. Under more auroral

20   conditions, the simple assumptions made in this study may not hold and the enhancement of gravity waves would likely distort the ionospheric profile. In addition, it appears that the observations are often made at high zenith angles at these latitudes, making them less useful both for interpreting the TIMED measurements but also in assuming dynamic equilibrium within the ionosphere. That is not to say that low-latitude ground-based ionospheric observations are without their own complications. Additional stratification, the F1.5 layer, can occur in this region (e.g. Yadav et al, 2012) while sporadic E and spread-F are

25   also commonplace. Despite these limitations, the station for which there were most coincident observations was at Kwajelein (9º N, 167ºE) situated within the Marshall Islands in the Pacific. Here there were 59 overpasses in total for which there were ground-based ionospheric data within 15 minutes and co-located within 5º latitude and longitude. Five of the ionospheric profiles were obscured by sporadic E (Es) while clear ionospheric profiles were apparent in the remaining 54. In order to increase the likelihood that the ionosphere was in a state of dynamic equilibrium, the data were further restricted to those for

30   which the solar zenith angle was less than 60º. The remaining 29 ionograms provided the best possible data set with which to compare ground-based observations with thermospheric profiles from the TIMED spacecraft while preserving a data set that was sufficiently large to ensure the comparison was meaningful.

5 Comparison between spacecraft and ionospheric data

In order to minimise the introduction of unconscious bias into the analysis, the height profile from each of the Kwajalein ionograms was manually scaled and the best-fit profile of the transition region was determined (through iteration of the model ionograms as detailed in section 3.2), without reference to TIMED data. Having fitted each of the ionograms, the scale height

5   at the F1 peak determined from the fit was used to estimate the thermospheric temperature. This temperature was in turn used to identify the altitude within the TIMED data from which the molecular to atomic concentration ratio was estimated. For the purposes of this analysis, this ratio was taken to be $[O]/([O_2]+[N_2])$. Any fit that resulted in an altitude of less than 125 km for the height of the F1 peak was deemed unphysical and removed from the analysis. This was the case for 4 of the traces which corresponded to ionograms for which a sporadic E layer or bifurcation of the E layer was seen.

10

As β is influenced by changes to thermospheric composition, a plot of $\sqrt{G}$ versus the molecular to atomic ratio should be linear. Such a plot is presented in figure 3 for the 25 cases used in this study. While there is some scatter, for the combination of reasons set out above, the data do indeed follow a linear trend, with a gradient of 2.23 ±0.17 and an offset of 1.66 ± 0.19.

6 Summary and discussion

15   It is apparent that this simple analysis has adopted many of the assumptions used during the analysis of King and Lawden (1964) and Rishbeth and Kervin (1968). From a modern perspective, more is now known about the temperature dependence of the loss rates pertinent to this study. Inclusion of this information, along with assumptions made about the rate of change of scale height with altitude, was prevented by a lack of independent temperature data. Were such information available (for example from co-located ground-based optical measurements of atmospheric airglow) these assumptions could be addressed.

20   Similarly the assumption that the ionospheric profile within the transition region is dominated by atomic ions will only be applicable to mid to low latitude stations under conditions of low geomagnetic activity. The presence of gravity waves and bifurcation of layers in ionograms can influence the shape of the trace and the visibility of the G parameter. These add scatter to the points plotted in figure 3. In particular, if there are additional layers apparent in the ionogram between the E and F1 peaks, this can lead to an underestimate of the scale height at the F1 peak, leading to an underestimate of the local temperature

25   and therefore the height of the F1 peak. Removing points which return an unrealistic height for hmF1 minimises the likelihood of such a systematic uncertainty influencing the fit of $\sqrt{G}$ versus the ratio of molecular:atomic concentrations.

Despite these simplifications, we have shown that there is a relationship between the G parameter estimated from ionograms and the thermospheric molecular:atomic concentration obtained from satellite data. While this result requires further validation

30   and there is much to do to advance the technique itself, it suggests that ground-based ionospheric data could be used to infer information about the neutral thermosphere. With the recent launch of the GOLD instrument (Eastes et al, 2017) there is further potential for detailed comparison of spacecraft measurements of the thermosphere with ground-based measurements of the

ionosphere. Calibrating these ground-based stations would enable investigation into the spatial scale of thermospheric variability as well as a quantitative method of studying long-term changes in thermospheric composition. Until now, such studies have been limited to qualitative comparisons (e.g. Rishbeth and Kervin, 1968, Scott, Stamper and Rishbeth, 2014, Scott and Stamper, 2015).

References

Aman, A. A. and Bman, B. B.: The test article, J. Sci. Res., 12, 135−147, doi:10.1234/56789, 2015.

15   Bremer, J.: Ionospheric trends in mid-latitudes as a possible indicator of the atmospheric greenhouse effect, J. Atmos. Terr. Phy., 54, 1505–1511, 1992.

Bremer, J.: Investigations of long-term trends in the ionosphere with world-wide ionosonde observations, Adv. Radio Sci., 2, 253-258, https://doi.org/10.5194/ars-2-253-2004, 2004.

Burnside, R. G., Herrero, F. A., Meriwether Jr., J. W., and Walker, J. C. G.: Optical Observations of Thermospheric Dynamics
20   at Arecibo, J. Geophys. Res., 86, 5532–5540, 1981.

Eastes, R.W., McClintock, W.E., Burns, A.G. et al.: The Global-Scale Observations of the Limb and Disk (GOLD) Mission, Space Sci Rev, 212: 383. https://doi.org/10.1007/s11214-017-0392-2, 2017.

Gardiner, G.W., Lane, J.A., Rishbeth, H.: Radio and Space Research at Slough 1920-1981, The Radio and Electronic Engineer, 52, 111-112, 1982.

25   Griffin, E. M., Aruliah, A. L., McWhirter, I., Yiu, H.-C. I., Charalambous, A., and McCrea, I.: Upper thermospheric neutral wind and temperature measurements from an extended spatial field, Ann. Geophys., 26, 2649–2655, 2008, http://www.ann-geophys.net/26/2649/2008/.

King, G. A. M.: Analysis of the F1-F2 transition region, J. Geophys. Res., 66, 2757-2762, 1961.

King, G. A. M.: The seasonal anomalies in the F region, J. Geophys. Res., 66, 4149-4154, doi: 10.1029/JZ066i012p04149,
30   1961b.

King, G. A. M., Seasonal changes in thermospheric composition, J. Atmos. Solar Terr. Phys., 32, 433-437, doi: 10.1016/0021-9169(70)90018-8, 1970.

King, G. A. M.: The validity of the "overlay" technique for analysing the F1-F2 transition, J. Atmos. Terr. Physics, 31, 515-529, 1969.

5   King, G. A.M., and Lawden, M.D.: Analysing the F-region with overlays, J. Atmos. Terr. Physics, 26, 1273-1280, 1964.

Kusnierkiewicz, D. Y., An overview of the TIMED spacecraft, John Hopkins APL Technical Digest, 24, 150-155, 2003.

Lawden, M. D.: Problems associated with overlay analysis of F1-region ionograms, J. Atmos. Terr. Phys., 31, 47-57, 1969.

Meier, R. R., et al: Remote Sensing of Earth's Limb by TIMED/GUVI: Retrieval of thermospheric composition and temperature, Earth and Space Science, 2, 1–37, doi: 10.1002/2014EA000035, 2015.

10 Meriwether, J. W., Tepley, C. A., Price, S. A., and Hays, P. B.: Remote Ground-Based Observations of Terrestrial Airglow Emissions and Thermospheric Dynamics at Calgary, Alberta, Canada, Optical Eng., 22, 128–131, 1983.

Nicolet, M.: Effects of the atmospheric scale height gradient on the variation of ionization and short wave absorption, J. Atmos. Terr. Phys., 1, 141-146, 1951.

Reinisch, B. W., and I. A. Galkin, Global ionospheric radio observatory (GIRO), Earth, Planets, and Space, 63, 377-381, doi:10.5047/eps.2011.03.001, 2011.

15 Rishbeth, H.: A greenhouse effect in the ionosphere?, Planet. Space Sci., 38, 945-948, 1990.

Rishbeth, H. and Kervin, C.:Seasonal changes displayed by F1-layer ionograms, J. Atmos. Terr. Physics, 30, 1657-1665, 1968.

Rishbeth, H. and Garriott, O.: An introduction to ionospheric physics, Pergamon Press, 1969.

Rishbeth, H., Roble, R. G.: Cooling of the upper atmosphere by enhanced greenhouse gases — modelling of thermospheric and ionospheric effects, Planet. Space Sci., 40, 1011-1026, 1992.

Rishbeth, H. and Setty, C. S. G. K.: The F-layer at sunrise, J. Atmos. Terr. Phys., 20, 263-276, doi: 10.1016/0021-9169(61)90205-7, 1961.

R.G. Roble, R.E. Dickinson: How will changes in carbon dioxide and methane modify the mean structure of the mesosphere and thermosphere?, Geophys. Res. Lett., 16, pp. 1441-1444, 1989.

25 Scott, C. J., Stamper, R., and Rishbeth, H.: Long-term changes in thermospheric composition inferred from a spectral analysis of ionospheric F-region data, Ann. Geophys., 32, 113-119, https://doi.org/10.5194/angeo-32-113-2014, 2014.

Scott, C. J. and Stamper, R.: Global variation in the long-term seasonal changes observed in ionospheric F region data, Ann. Geophys., 33, 449-455, https://doi.org/10.5194/angeo-33-449-2015, 2015.

Shimizaki, T.: On the continuity equation for electron density in the ionosphere, J. Atmos. Terr. Physics, 27, 593-604, 1965.

30 Storey, L. R. O.: The joint use of the ordinary and extraordinary virtual height curves in determining ionospheric layer profiles, J. Geophys. Res., 64D,111-124, 1960.

Spencer, N. W., and Carignan, G. R.: In Situ Measurements of Thermospheric Composition, Temperature and Winds by Mass Spectrometry, Adv. Space Res. Vol. 8, No. 5—6, pp (5)107—(5)117, 1988.

Annales
Geophysicae
Discussions

International Geomagnetic Reference Field: the 12th generation, Erwan Thébault, Christopher C Finlay, Ciarán D Beggan, Patrick Alken, Julien Aubert, Olivier Barrois, Francois Bertrand, Tatiana Bondar, Axel Boness, Laura Brocco, Elisabeth Canet, Aude Chambodut, Arnaud Chulliat, Pierdavide Coïsson, Francois Civet, Aimin Du, Alexandre Fournier, Isabelle Fratter, Nicolas Gillet, Brian Hamilton, Mohamed Hamoudi, Gauthier Hulot, Thomas Jager, Monika Korte, Weijia Kuang, Xavier

5   Lalanne, Benoit Langlais, Jean-Michel Léger, Vincent Lesur, Frank J Lowes et al. Earth, Planets and Space 2015, 67:79, 2015.

Yadav, S., Upadhayaya, A. K., and Das, R. M.: Daytime additional F layer stratification over low-midlatitude

station of the Indian sector under geomagnetic disturbed conditions, J. Geophys. Res., 117, doi:10.1029/2011JA017305, 2012.

Yee, J-H, et al: TIMED instruments, John Hopkins APL Technical Digest, 24, 2003.
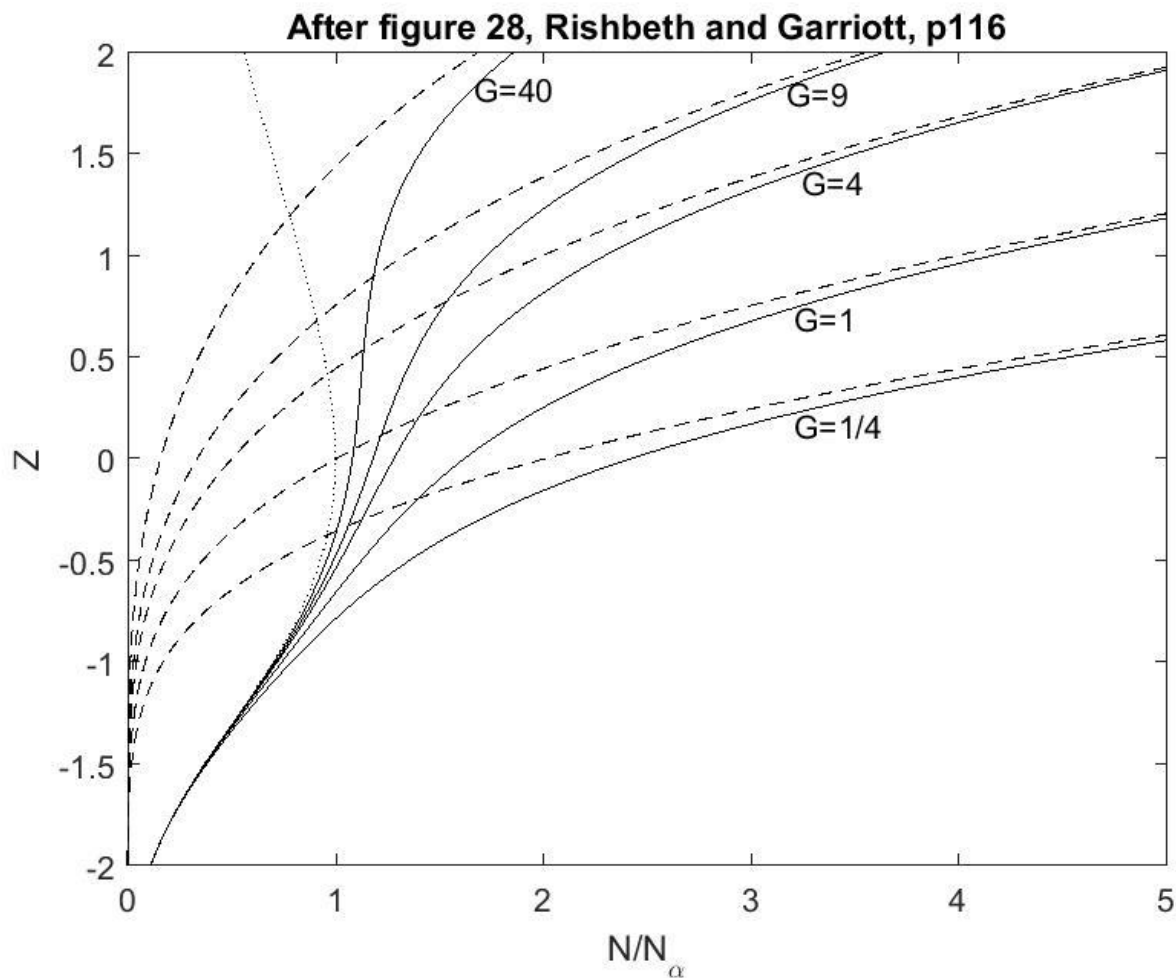
10

Figure 1: Electron concentration versus reduced height for the ionospheric transition region. For a Chapman production function, q(z) with peak at z=0 and a square-law loss coefficient, α. A linear loss coefficient, β=β₀exp(-1.75z) is used, with five values of β₀

representing G values of ¼, 1, 4, 9 and 40. The dashed lines represent $N_\beta = q/\beta$. The dotted line represents $N_\alpha = (q/\alpha)^{1/2}$. The solid lines are the profiles N(z) calculated from equation (7), scaled by $N_{\alpha 0} = (q_0/\alpha)^{1/2}$. The F1 ledge is most pronounced for G=40 and absent for G=¼.
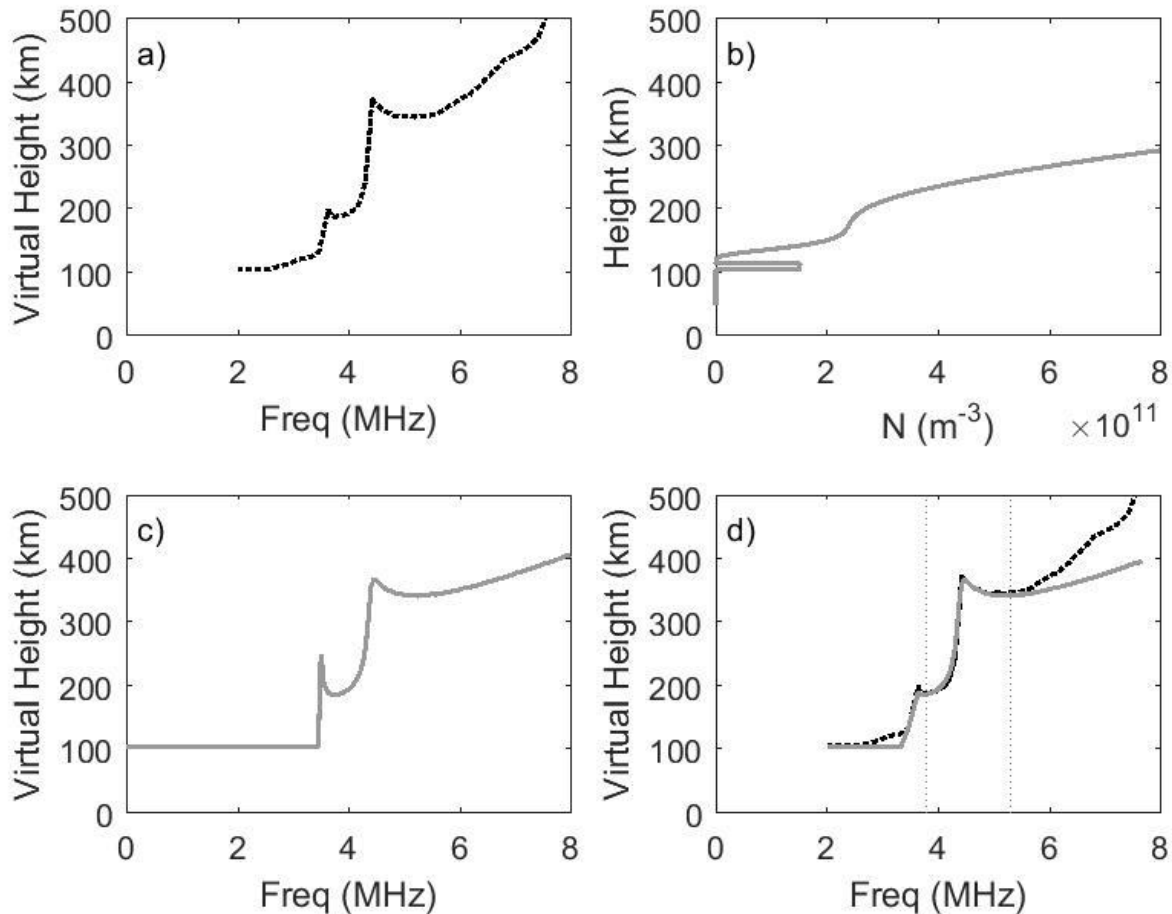
Figure 2: An example of the fitting procedure. The virtual height profile is manually scaled from an ionogram (a). The five fit parameters are then iterated to create an electron concentration profile (b) which is in turn inverted to create an artificial ionogram (c). The values of the variables are iterated until the residual is minimised between the real and model ionograms (d). The comparison between the model ionogram (grey) and the real ionogram is only valid in the transition region (indicated by the two vertical dotted lines) and so only the data between these lines are considered when calculating the minimum residual.
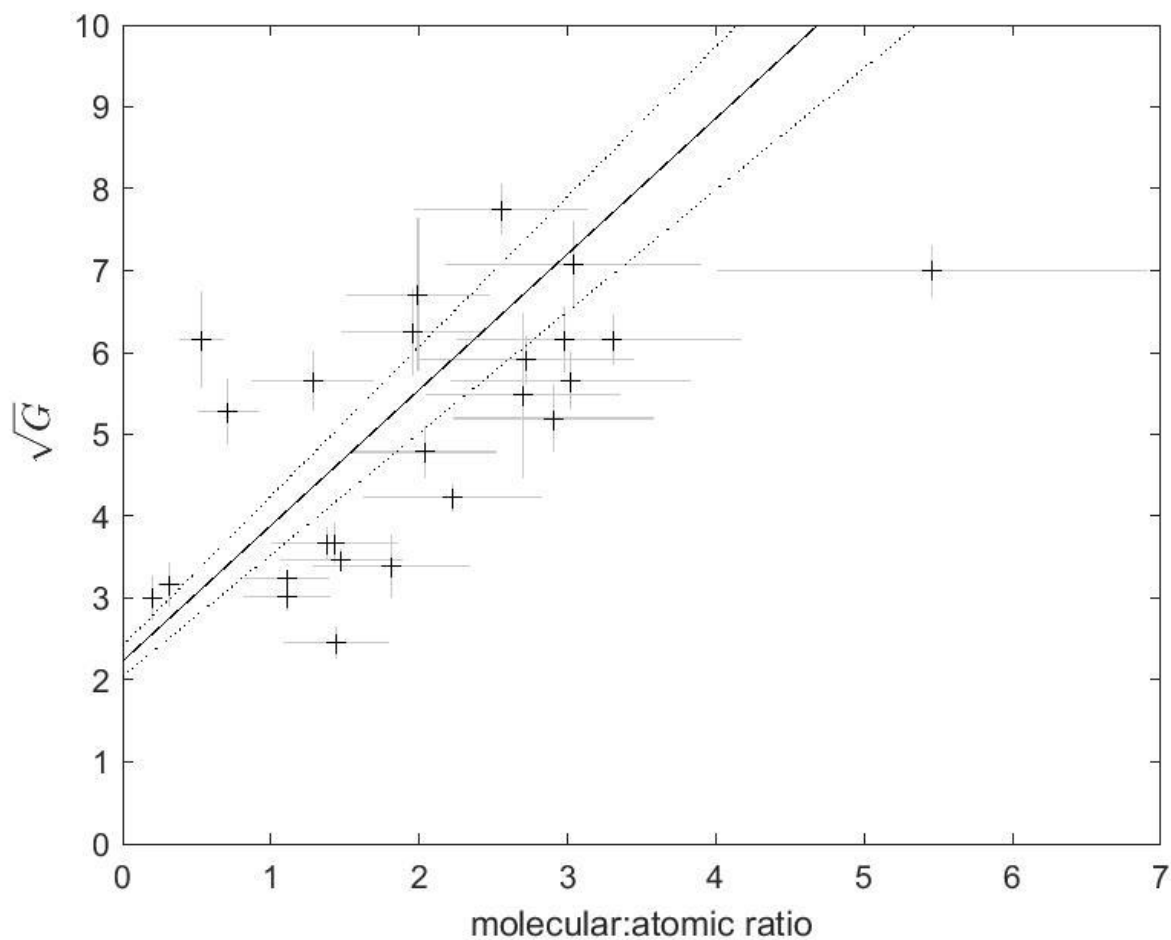
Figure 3: A plot of √G (obtained from the model fit to ionograms) versus the thermospheric molecular:atomic ratio calculated from the associated TIMED neutral density profile. For each data point, the fitted scale height at the F1 peak was used to estimate the thermospheric temperature. This was then used to identify the appropriate height at which to interpolate the thermospheric composition ratio from the TIMED dataset. The solid line represents a weighted linear least-squares fit to the data while the dotted lines represent the uncertainty in the fit parameters.